Influence of initial geometric imperfections on the stability of thick cylindrical shells under internal pressure

Stefane Lopes, Paul Gonçalves, Djenane Pamplona

Influence of initial geometric imperfections on the stability of thick cylindrical shells under internal pressure

S. R. X. Lopes, P.B.Gonçalves, and D. C. Pamplona

Civil Engineering Department, Pontifical Catholic University, Brazil

This paper investigates numerically and experimentally the influence of initial geometric imperfections on the critical loads of initially stretched thick hyperelastic cylindrical shells under increasing uniform internal pressure. Imperfections in shells can have a global or local character. First, two types of local imperfections are considered: (1) a local axially symmetric imperfection in the form of a ring and (2) a small rectangular imperfection. The influence of the imperfection thickness, position and size are analysed in detail. Results show that the critical load decreases as the imperfections increase in size or thickness and as they move from the boundaries to the centre of the shell. The influence of multiple local imperfections is also studied in the present paper. Finally, the influence of global imperfections is considered with the imperfections described as a variation of the shell curvature in the axial direction. The results show that thick hyperelastic shells may be sensitive to local and global imperfections. In all cases the experimental results are in good agreement with the numerical ones, corroborating the conclusions.

1. INTRODUCTION

In previous works [1, 2] the authors studied the non-linear behaviour and instability of thin cylindrical shells and carried out a detailed numerical and experimental parametric analysis of these shells. As the imperfections of these test specimens were small, a good agreement between the experimental and numerical results was obtained. However, the initial geometric imperfections may have a marked influence on the behaviour of this type of structure, as it happens in the analysis of thin metal cylindrical shells. Koiter [3] was the first one to develop a theory that explains in a rational form, based on the influence of imperfections, the discrepancy between theoretical and experimental results in the buckling analysis of certain structures. Amongst them, axially compressed cylindrical shells and spherical shells submitted to external pressure stand out. The theory of Koiter allows the determination of the type of bifurcation that occurs at the first bifurcation point along an equilibrium path and the verification of its sensitivity to initial geometric imperfections.

Thick shells submitted to large elastic deformations under the action of increasing internal pressure can display global and local instabilities. Initially, when submitted to internal pressure, the shell deforms almost uniformly throughout its length (except near the boundaries). After a certain critical pressure is reached, a bulb appears in the shell. This instability is followed by a sudden decrease of the internal pressure and a decrease in the radial deformation of the other parts of the structure. This instability corresponds to a limit point along the non-linear equilibrium path, that is, a turning point of the surface tension that corresponds to a bifurcation point. In a perfect shell, the bulb has an axi-symmetrical form and occurs in the middle of the shell. This behaviour is known in literature as localization [4] and was observed in thick hyperelastic membranes by Kyriakides and Chang [5], who analysed this problem both theoretically and experimentally. However, due to imperfections, the bulb can occur in any place along the length of the shell and may become completely asymmetrical. This behaviour can be observed in different areas of study, with the formation of aneurisms being one of the most important (Figure 1).

The linear constitutive laws valid for the small strain regime are sometimes extended to the large displacement, small strain, which can lead to unrealistic results when large deformations are

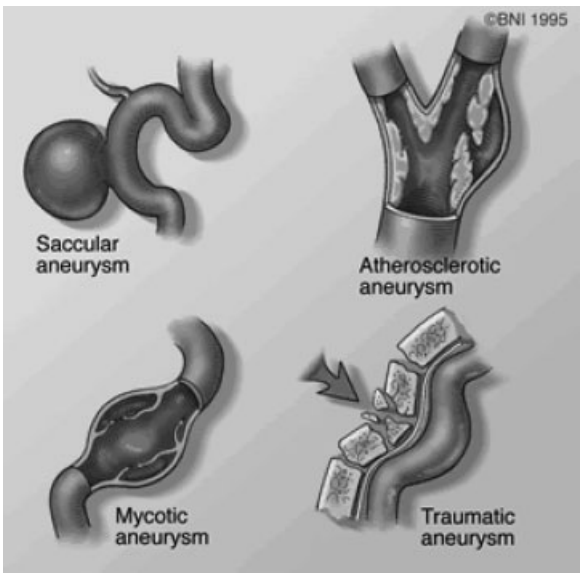

Figure 1. Cerebral aneurisms (Barrow Neurological Institute Web site).

present. In such cases, elasticity in the fully non-linear range must be employed. The pioneering work of Green and Adkins [6] on non-linear elasticity set up the basis for the analysis of structures under large deformations. Historically, the large deformations observed in rubber-like materials under several loading conditions motivated researchers to express the associated non-linear elastic behaviour through hyperelastic models. Among the hyperelastic models, strain invariant based Mooney–Rivlin model [7, 8] is the oldest one. The simplest constitutive model is the Neo-Hookean model, which can be viewed as a simplification of the Mooney–Rivlin law. The analysis of thin hyperelastic cylindrical shells has been a problem of continued interest. The investigation of the equilibrium and stability of thin cylindrical tubes under uniform pressure loading or loads acting along the boundaries has been examined theoretically, for instance, by Alexander [9], Ratner [10], Haseganu and Steigmann [11], Haughton [12] and Gent [13]. Experimental investigations were carried out by Pamplona and Bevilacqua [14] and Pamplona *et al*. [1, 2], among others. When the thickness to the outer radius ratio is small, it can be modelled as an ideal membrane subjected only to in-plane normal and shearing forces. When the membrane becomes thicker, flexural effects cannot be disregarded in the analysis and the structure must be modelled as a shell or a solid. The analysis of large deformations of hyperelastic thick shells is not so popular, nevertheless there are some important publications such as the ones by Kyriakides and Chang [5] and, more recently, the works by Tang *et al*. [15] and Haussy and Ganghoffer [16] where the theory of thick hyperelastic shells was used for modelling carotid arteries and aneurysms, respectively. An analytical solution for a perfect elastic thick tube under axial load was presented by Haughton and Ogden [17].

In this work the imperfection sensitivity of thick hyperelastic shells under internal pressure is analysed numerically and experimentally. To the authors knowledge this is the first work where the effect of large local imperfection in thick hyperelastic shells is analysed in detail. Non-symmetrical and axi-symmetrical local and global imperfections are considered in the analysis. The effect of multiple local imperfections is also investigated. Variations of the imperfection thickness, length and position along the shell length are considered. In the theoretical formularization of the problem, the material of the shell is considered to be incompressible, homogeneous and isotropic and modelled as a Mooney–Rivlin material, which is described by two elastic constants. These assumptions are sufficiently reasonable when compared with the physical behaviour of the shell used in the experimental analysis (a latex shell). In the analysis of the large deformations of the shell, the non-linear shell response is obtained by the finite element code ABAQUS [18, 19]. This code offers a good library of non-linear finite elements and constitutive laws for analyses of shells under large deformations. Newton–Raphson algorithm is used together with Riks arc-length method to obtain the post-critical behaviour of the shell under traction and internal pressure. In the experimental analysis, two types of imperfections are considered: the first one, an axi-symmetrical imperfection in the form of a ring, and then in the form of a small square. In all the cases a good qualitative agreement is observed between the numerical and experimental analysis. Since one of the main influences on the formation of aneurysms is the presence of local imperfections due to variations in the wall thickness, we feel that the present work is a useful contribution in this area.

2. ANALYSIS OF AXI-SYMMETRICAL IMPERFECTIONS

2.1. Experimental analysis

The numerical results are conducted considering latex shells with undeformed radius R, length L and thickness H. The material of the shell is considered, based on experimental results, as

homogeneous, isotropic and incompressible [20]. Its geometric characteristics were measured by the Institute of Metrology of the Catholic University of Rio de Janeiro (ITUC—PUC-Rio) and the results are presented in Table I.

The local imperfection has the form of a ring, as illustrated in Figure 2. It is generated, with the aid of an electric sander, by the reduction of the thickness of the shell. It must be pointed out that it is very difficult to control the thickness of the shell in the imperfection region. In the tested specimens, the wall thickness was reduced between 40 and 50%. The imperfect shell initially is under traction through an imposed axial displacement ΔL with a relation $\Delta L/L = 0.16$. After the initial elongation, the shell is fixed in its two extremities. Then it is gradually filled with air. The imperfection has length L_{imp}, thickness H_{imp} and is located at a distance Z_i from the upper edge. Five different values of Z_i are considered, as shown in Table II.

The results of these five experiments are shown in Figure 3, where, for each imperfection, the critical configuration (formation of the bulb or aneurysm) and the respective value of the measured critical pressure P_{cr} (10^{-2} MPa) is shown.

For imperfections located in positions Z_1 and Z_2, the bulb does not occur in the place of the local imperfection. This shows that even large imperfections near the supports do not interfere with the localization of the bulb. However, for imperfections far from the supports (Z_3 to Z_5)

Table I. Geometric characteristics of the latex shell used in the experimental analysis.

	External radius	Thickness	Length	Geometric relations	
Rubber	R(mm)	H(mm)	L(mm)	R/H	L/R
Latex	9.38	3.58	200.00	2.63	22

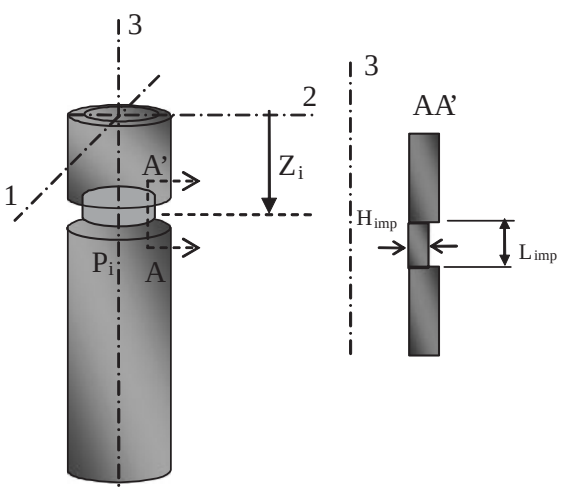

Figure 2. Geometry of the axi-symmetric imperfection.

Table II. Position of the ring imperfection.

Position of the imperfection	Position from the superior support (%L)
Z_1	$0.02L$
Z_2	$0.05L$
Z_3	$0.20L$
Z_4	$0.30L$
Z_5	$0.45L$

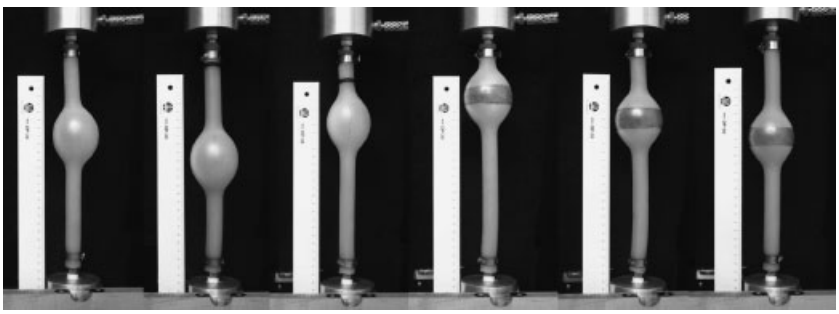

(a) P_{cr} = 11.8 (b) P_{cr} = 11.98 (c) P_{cr} = 11.67 (d) P_{cr} = 11.43 (e) P_{cr} = 11.3 (f) P_{cr} = 11.33

Figure 3. Critical configurations, obtained experimentally, and the corresponding critical pressures: (a) perfect shell and shell with imperfection at (b) $Z_1 = 0.02L$; (c) $Z_2 = 0.05L$; (d) $Z_3 = 0.20L$; (e) $Z_4 = 0.30L$; and (f) $Z_5 = 0.45L$.

the bulb appears exactly in the place where the imperfection was generated, as observed in the photographs. When the imperfection is near the support, the place of the buckling localization is influenced by other small imperfections that may exist in the specimen. As observed, even for the so-called perfect shell, the bulb does not occur in the middle, as expected from symmetry conditions for a perfect shell. The theory can, of course, be rewritten to force the bulb to appear anywhere along the shell.

Figure 4 shows the variation of the critical load with the distance of the imperfection from the upper support, Z_i. Initially, a small increase in the critical pressure occurs (position Z_1), followed by a decrease of the critical pressure for the other four imperfection positions. This is also observed numerically, as it will be shown in the next section.

2.2. Numerical analysis

Analytical studies of thin hyperelastic shell can be conducted only for simple geometries and loading cases [9–14]. For thick hyperelastic shells even simple problems can rarely be treated theoretically [17]. So, for most of the problems related to real hyperelastic shells, the solutions are usually obtained through numerical techniques. The most used methodology is the finite element method. However, for a correct analysis a shell element appropriate for large deformation analysis and a proper constitutive law for hyperelastic materials are required. Here, the numerical study is carried out using the finite element program ABAQUS. The shell has the same geometry as the one used in the experiments (Table I).

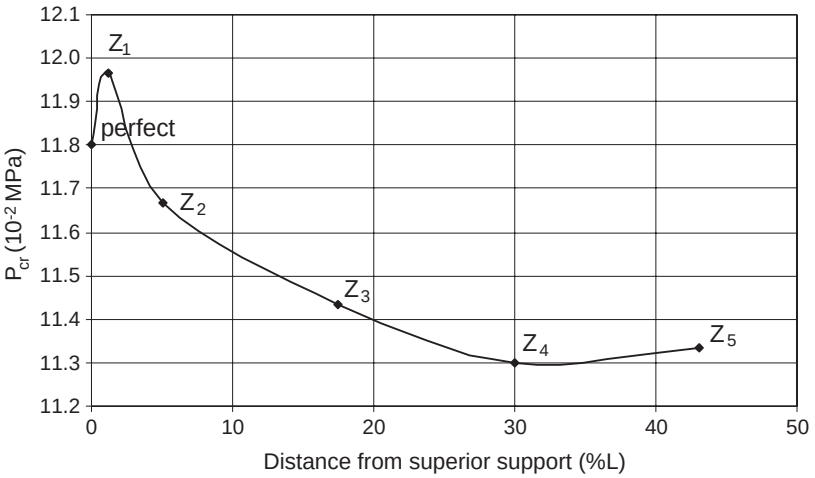

Figure 4. Variation of the critical pressure with the localization of the imperfection ring.

Isotropic hyperelastic materials are conveniently represented in terms of a strain energy density w. Assuming the complete recoverability after deformation, the strain energy density depends only on the final state of strain and not on the loading. Thus given an undeformed reference state, the strain is characterized by the principal stretches λ_1 (meridional), λ_2 (azimuthal) and λ_3 (transversal) or, alternatively, by the strain invariants I_1, I_2 and I_3, that is

$$w = w(\lambda_1, \lambda_2, \lambda_3) = w(I_1, I_2, I_3) \tag{1}$$

The three strain invariants of the deformation field are given by

$$\begin{aligned} I_1 &= \mathbf{g}^{ij}\mathbf{G}_{ij} \\ I_2 &= \mathbf{G}^{ij}\mathbf{g}_{ij}\, I_3 \\ I_3 &= \frac{G}{g} \\ G &= |\mathbf{G}_{ij}|, \quad g = |\mathbf{g}_{ij}| \end{aligned} \tag{2a}$$

where $\mathbf{G}^{ij}$ and $\mathbf{g}^{ij}$ are the contravariant components of the metric tensors of the undeformed and deformed states, respectively, and $\mathbf{G}_{ij}$ and $\mathbf{g}_{ij}$ are the corresponding components of the covariant metric tensor [6].

The three deformation invariants can be rewritten in terms of the principal stretches λ_i $(i = 1, 2, 3)$ as

$$\begin{aligned} I_1 &= \lambda_1^2 + \lambda_2^2 + \lambda_3^2 \\ I_2 &= (\lambda_1\lambda_2)^2 + (\lambda_2\lambda_3)^2 + (\lambda_1\lambda_3)^2 \\ I_3 &= (\lambda_1\lambda_2\lambda_3)^2 \end{aligned} \tag{2b}$$

Volume changes in rubber-like materials are very small, as shown by Treolar [21], and the simplifying assumption of incompressibility is usually adopted. Thus the constraint

$$I_3 = 1 \tag{3}$$

is identically satisfied throughout the material. The strain energy density is then considered as a function of I_1 and I_2 only. Hence, the theoretical representation of the behaviour of a hyperelastic incompressible material is given by the definition of the function $w(I_1, I_2)$.

There are several constitutive laws in literature particularly adapted to the representation of elastomers. Rivlin [8] has proposed the following polynomial form for the energy density function:

$$w = \sum_{m,n} C_{mn}(I_1 - 3)^m (I_2 - 3)^n \tag{4}$$

also known as the Mooney–Rivlin strain energy density function because the first-order polynomial function

$$w = C1(I_1 - 3) + C2(I_2 - 3) \tag{5}$$

has first been introduced by Mooney [8]. Equation (5) is a function of two constants, $C1$ and $C2$. This is probably one of the most used density functions in finite element codes.

A simplified form of Equation (5)

$$w = C1(I_1 - 3) \tag{6}$$

known as the Neo-Hookean strain density function, has also been extensively used in literature.

Here, the shell material is modelled as a hyperelastic material of the Mooney–Rivlin type with elastic constants $C1 = 0.100398$ MPa and $C2 = 0.150843$ MPa. These constants were obtained experimentally for this material by Xavier [20], and a good agreement was observed between experimental and numerical tests. The experimental methodology can also be found in Pamplona *et al.* [1, 2].

2.2.1. Influence of the position of the local imperfection—Z_i. First, a convergence analysis of the mesh used with elements of type S4R (quadrilateral shell elements with reduced integration) is conducted. It is observed that a good convergence is attained for the critical load for a number of elements more than 1340. Therefore, all analyses are carried out using 1992 shell elements of type S4R.

The local imperfection position (Z_i) varies from $0.02L$ to $0.45L$ in relation to the lower support of the shell (see Table II). The ring imperfection has thicknesses that vary from $H_{\text{imp}} = 1.5$ to 3.0 mm, that is, from $H_{\text{imp}} = 0.40H$ to $0.85H$, with H being the thickness of the undeformed shell. For the imperfection length two values are considered: $L_{\text{imp}} = 5$ mm and $L_{\text{imp}} = 0.025L$, where L is the undeformed length of the shell.

Figure 5 shows the variation of the internal pressure as a function of the maximum radial displacement, U_r, for different positions of the ring imperfection, as well as the response of the perfect shell. The influence of the imperfection on the bifurcation load is small and decreases as the imperfection approaches the support, as shown in Figure 5(b).

Figure 6 shows the critical configuration for each case. It is observed that, for an imperfection of thickness $H_{\text{imp}} = 0.85H$, in positions Z_1 and Z_2 (Figure 6(a) and (b)), the formation of the bulb occurs, as for the perfect shell, in the middle of the shell. However, for positions Z_3, Z_4 and

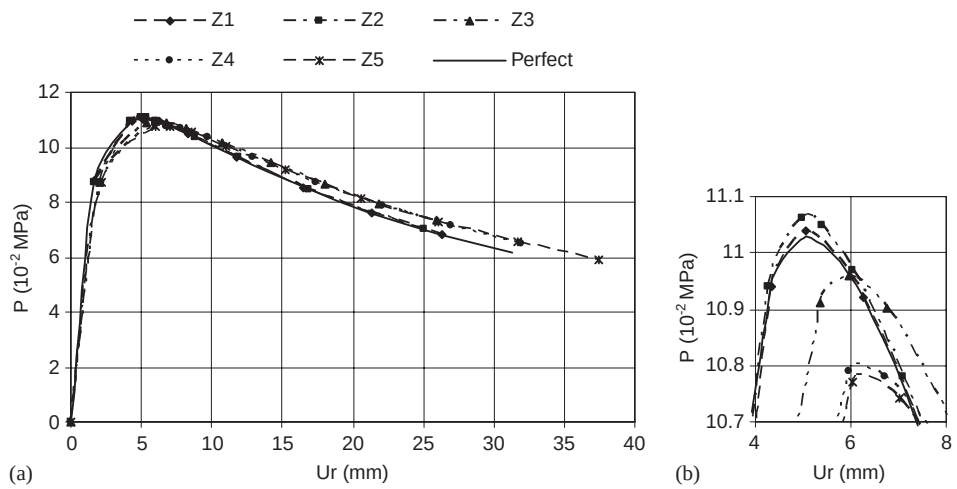

Figure 5. (a) Internal pressure as a function of the maximum radial displacement for different positions of the imperfection (Z_i); and (b) the detail of the region of the maximum pressures.

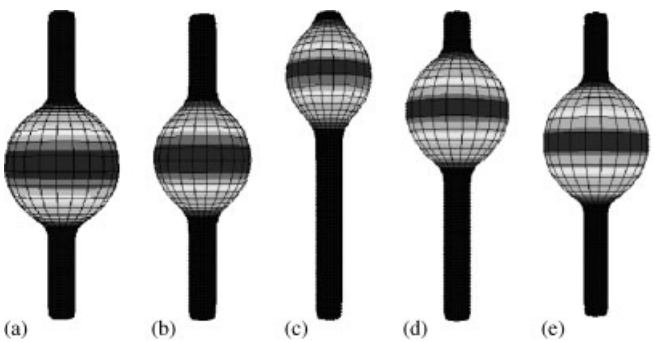

Figure 6. Deformed cylindrical shell with imperfection thickness $H_{\text{imp}} = 0.85H$, for imperfection in positions Z_1–Z_5: (a) $Z_1 = 0.02L$; (b) $Z_2 = 0.05L$; (c) $Z_3 = 0.20L$; (d) $Z_4 = 0.30L$; and (e) $Z_5 = 0.45L$.

Z_5 (Figures 6(c)–(e)), the bulb appears at the position of the imperfection ring (the imperfection in the middle of the bulb). This agrees with the general behaviour observed in the experimental analysis.

Figure 7 shows the variation of the critical pressure with the position of the imperfection for different imperfection thicknesses. There is a small increase in the critical pressure for positions Z_1 and Z_2 when compared with the perfect shell when the thickness of the imperfection is between zero and $0.85H$ (see detail in Figure 7(b)). These imperfections are close to one of the supports. However, for smaller imperfection thicknesses, this increase occurs solely for position Z_1. As the distance of the imperfection from the support increases, the critical pressure decreases. This decrease is also followed by a change in the localization of the bulb, as observed previously (Figure 6).

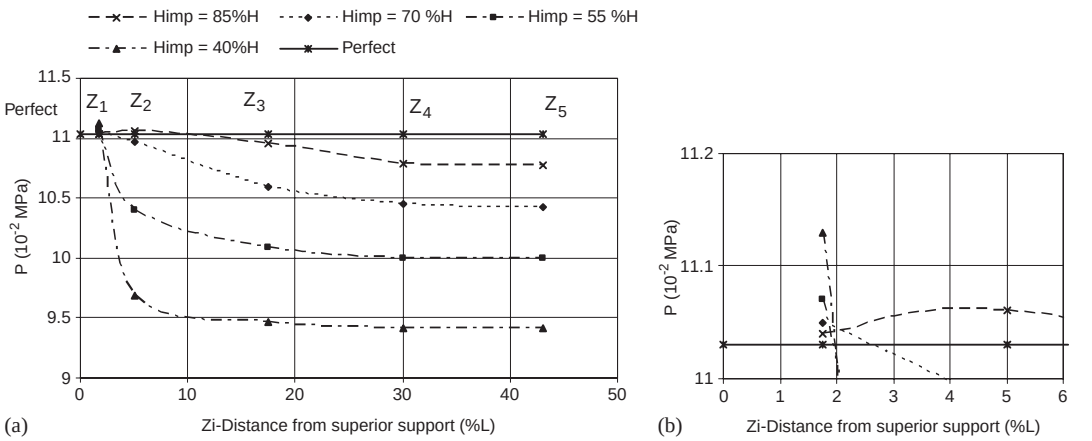

Figure 7. (a) Variation of the critical pressure with the position of the imperfection for different values of the imperfection thickness; and (b) detail near position Z_1.

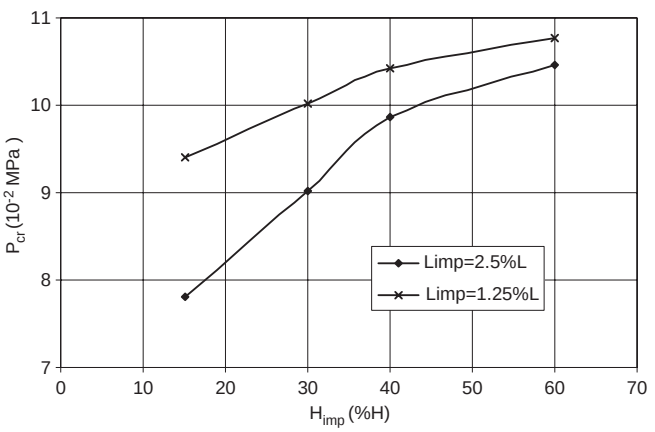

Figure 8. Variation of the critical pressure as a function of the thickness of the shell for two lengths of imperfection: $0.0125L$ and $0.0250L$.

2.2.2. Effect of the variation of the thickness and length of the local imperfection. Consider again the same shell submitted to the same traction level and under increasing internal pressure. Here the influence of the variation of thickness and length of the imperfection ring are analysed for an imperfection located in position Z_5 (Table II). This is the most sensitive location for the imperfection, as shown previously. Two lengths of the imperfection are considered: $L_{\text{imp}} = 0.0125L$ and $L_{\text{imp}} = 0.0250L$. The thickness of the imperfection varies from $0.45H$ to $0.85H$. Figure 8 shows the variation of the critical pressure with the thickness of the shell for the two distinct lengths of imperfection. One notices that, as expected, the critical pressure of the shell is directly proportional to the thickness of the imperfection, but inversely proportional to its length of the imperfection.

Now the effect of length variation for imperfections located in positions Z_2 and Z_5 is analysed, considering $H_{\text{imp}} = 0.85H$. The length of the imperfection varies from $0.0125L$ to $0.05L$. Figure 9

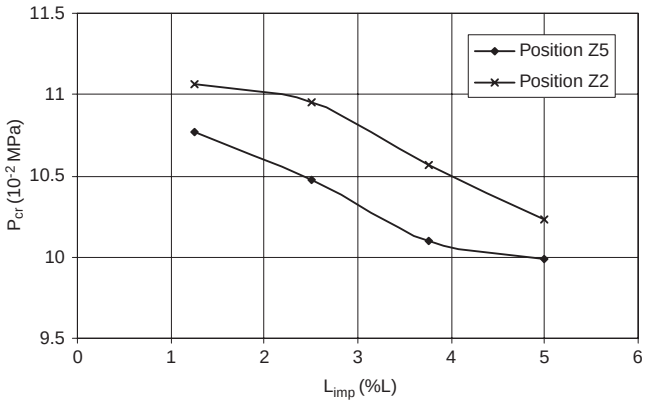

Figure 9. Variation of the critical load with the increase of the length of the ring of imperfection for 2 positions Z_2 and Z_5.

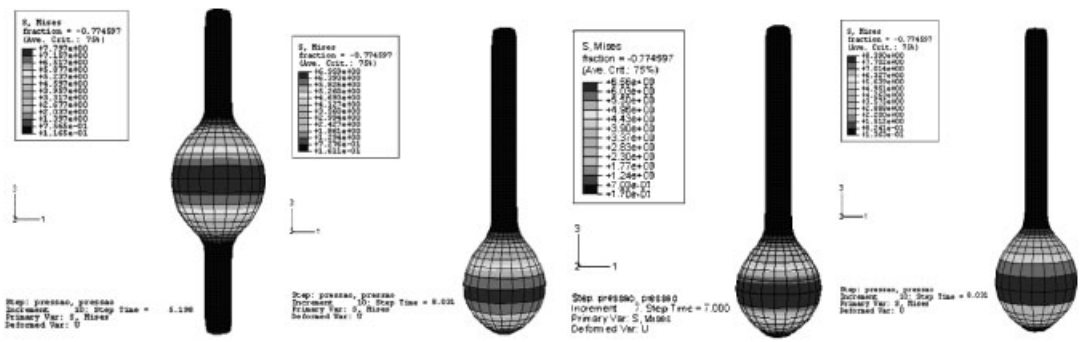

$L_{imp} = 0.0125L$ $L_{imp} = 0.025L$ $L_{imp} = 0.0375L$ $L_{imp} = 0.05L$

Figure 10. Critical configuration of the shell with imperfection at position Z_2 for lengths of imperfections varying between $0.0125L \leqslant L_{\text{imp}} \leqslant 0.05L$.

presents the variation of the critical load with the increase of the length of the imperfection. As the imperfection length increases, the critical load decreases and approaches a lower bound.

For position Z_2, the bulb appears initially in the central region of the shell. However a change in the localization of the bulb occurs for imperfection lengths of $0.025L$ or higher (Figure 10). However, for position Z_5, the bulb appears at the position of the imperfection for all the considered imperfection lengths.

3. STUDY OF THE LOCAL GEOMETRIC IMPERFECTIONS IN A SQUARE SHAPED REGION

3.1. Experimental analysis

Again, for the same shell geometry experiments considering shells with imperfections in the form of a small square along the length of the shell are carried out. These imperfections also are

generated with the aid of an electric sander, through the reduction of the thickness of the shell, with dimensions of $0.025L \times 0.025L$. It must be pointed out that it is very difficult to control the thickness of the shell in the imperfection region. The critical configurations for imperfections at positions Z_1–Z_4 are presented in Figure 11.

Figure 12 shows the variation of the critical pressure with the position of the imperfection. One notices that, for all the imperfection positions, a small decrease of the critical pressure occurs. However, the critical load for position Z_2 is slightly higher than that of position Z_1. After this local maximum, the pressure decreases as the distance of the imperfection from the support increases. This fact, although puzzling, since the imperfection is actually strengthening the tube, was observed both numerically and experimentally. For positions Z_1 and Z_2 the bulb position is not affected by the imperfection, while for positions Z_3 and Z_4 the bulb appears exactly at the position of the imperfection. A behaviour similar to that observed experimentally for the axi-symmetric imperfection.

(a) P_{cr} = 11.43 (b) P_{cr} = 11.5 (c) P_{cr} = 11.32 (d) P_{cr} = 11.28

Figure 11. Experimental results. Critical configurations for shells with initial imperfection in a square shaped region in positions: (a) $Z_1 = 0.02L$; (b) $Z_2 = 0.05L$; (c) $Z_3 = 0.20L$; and (d) $Z_4 = 0.30L$.

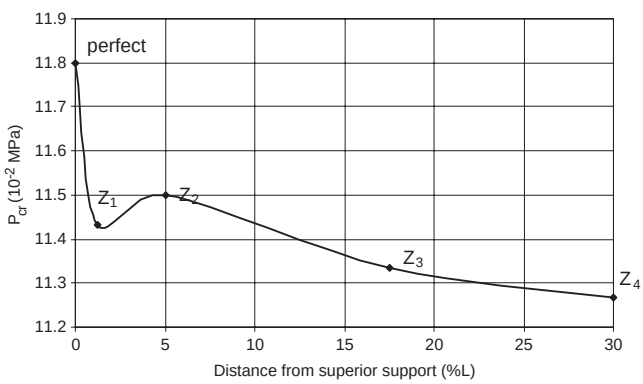

Figure 12. Variation of the experimental critical pressure with the position of the imperfection.

3.2. *Numerical analysis*

Now a numerical investigation of the behaviour of the imperfect shell is conducted. The local imperfection is represented by the reduction of the thickness of the shell in a square shaped region with dimensions of $0.025 \times 0.025L$ and variable thickness. The variation of the position of the imperfection along the length of the shell is the same one adopted in the previous item (Z_1, Z_2, Z_3 and Z_4).

The convergence analysis carried out in the previous item also applies to this analysis. Thus, as in the previous analysis, a mesh with 1992 S4R elements and 2016 nodes is considered. The results, shown in Figure 13, exhibit a small variation of the critical pressure with the position of the imperfection. In this case the imperfection thickness is $H_{\text{imp}} = 0.85H$. Figure 14 illustrates the critical configurations obtained numerically. As in the experimental analysis, for imperfection Z_1 and Z_2 the bulb position is not affected by the imperfection, while for positions Z_3 and Z_4 the bulb appears exactly at the position of the imperfection. Also it is observed for positions Z_3

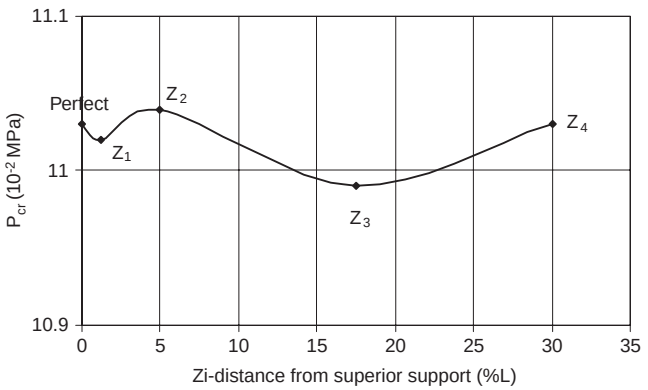

Figure 13. Variation of the critical pressure with the position of the imperfection ($H_{\text{imp}} = 0.85H$).

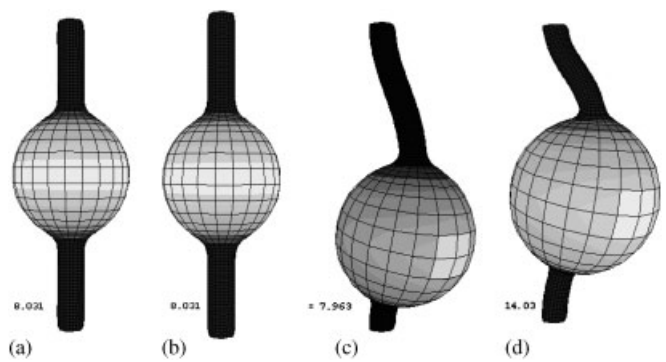

Figure 14. Deformed configurations of shells with local imperfections of dimensions $0.025L \times 0.025L \times 0.85H$ for positions Z_1–Z_4: (a) $Z_1 = 0.02L$; (b) $Z_2 = 0.05L$; (c) $Z_3 = 0.20L$; and (d) $Z_4 = 0.30L$.

and Z_4 a loss of symmetry that affects the global behaviour of the shell. In addition to the local instability, a global, column type instability occurs.

Now the same shell with an imperfection of thickness $H_{\text{imp}} = 0.75H$ is studied. The variation of the critical pressure as a function of the imperfection position is shown in Figure 15. For this imperfection thickness the critical pressure is different from the previous case (Figure 13). Here a small increase of the critical pressure in relation to the perfect shell occurs for Z_2. However, for the other positions, the critical pressure decreases, being this decrease more significant in position Z_1. As illustrated in Figure 16, for an imperfection in positions Z_1, the bulb develops in the middle of the shell. For the other imperfection positions the bulb appears in the place of the imperfection. Again, a loss of symmetry of the deformed shell for these imperfection positions is observed.

In order to understand the effect of the imperfection thickness on the critical load and mode, a shell with $H_{\text{imp}} = 0.55H$ is now analysed. Again, as shown in Figure 17, a small variation of the critical pressure in relation to the one of the perfect shell is observed. From these results, one can conclude that the imperfection thickness and position has only a small influence on the

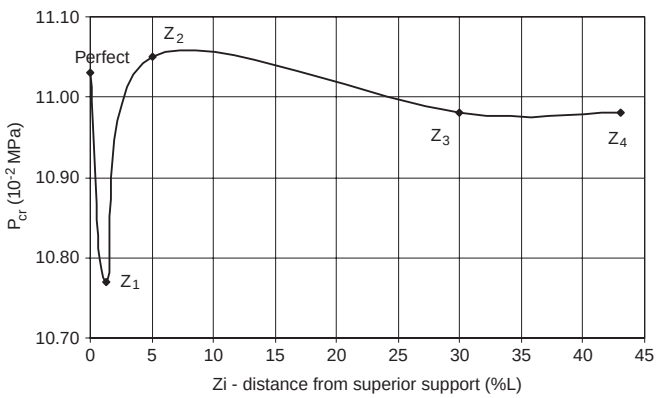

Figure 15. Variation of the critical pressure with the position of the imperfection of dimensions $0.025L \times 0.025L \times 0.75H$.

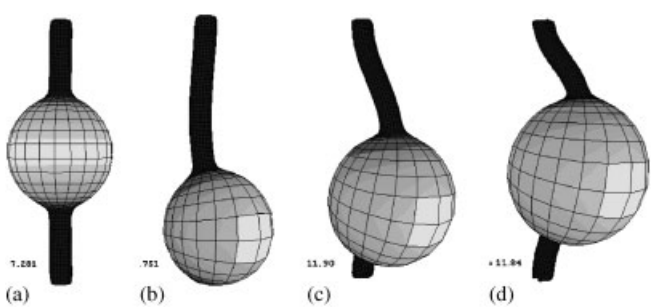

Figure 16. Configurations of the shell at the critical points with an imperfection of dimensions $0.025L \times 0.025L \times 0.55H$ in positions Z_1–Z_4: (a) $Z_1 = 0.02L$; (b) $Z_2 = 0.05L$; (c) $Z_3 = 0.20L$; and (d) $Z_4 = 0.30L$.

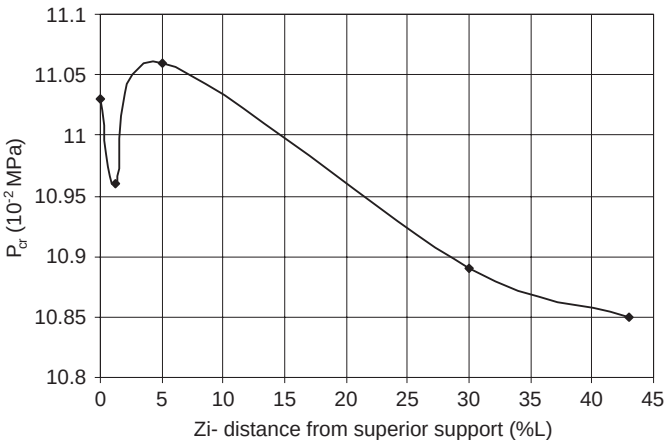

Figure 17. Variation of the critical pressure with the position of the imperfection for $H_{\text{imp}} = 0.55H$.

critical pressure. However the variation of this critical pressure, although small, is different for different values of the imperfection thickness. On the other hand, the imperfections have an important influence on the local and global instability mode of the shell.

4. STUDY OF MULTIPLE LOCAL GEOMETRIC IMPERFECTIONS

Here two imperfections, equidistant from the supports and forming an angle θ_{imp} between them, are considered. The angle θ_{imp} varies from 0° to 180°, as illustrated in Figure 18. As in the previous analysis, the imperfections have the form of a small square and are considered to have the same geometry. The analysed shells have 3 mm thicknesses, 400 mm length, and 11 mm diameter ($H/R = 0.55$ and $L/R = 72.7$). The imperfections are located $0.05L$ from the supports (position Z_2, as presented in Table II) and two imperfection thicknesses are considered, namely $H_{\text{imp}} = 0.55$ and $0.75H$.

Again a convergence analysis was carried out and it was observed that 1500 S4R elements are sufficient to obtain a good convergence for all configurations. Based on this analysis, a mesh of 1688 S4R elements and 1656 nodes is adopted.

Figure 19 shows the obtained critical configurations for $\theta_{\text{imp}} = 0°$. The imperfections have thicknesses of $H_{\text{imp}} = 0.55$ and $0.75H$ and are located at a distance of $0.05L$ from the supports. It is observed in the Figure 19(a) that, for an imperfection thickness $0.55H$, the shell does not exhibit a global instability, with instabilities concentrated in the regions of the imperfections. However, as shown in the Figure 19(b), for an imperfection thickness of $0.75H$, besides the two local instabilities, a global instability mode is observed. Figure 19(c) shows the typical non-linear behaviour of a hyperelastic thick shell under traction and increasing internal pressure. As expected, the critical load decreases as the thickness of the imperfection decreases.

The influence of the angle between the two imperfections is studied by varying θ_{imp} from 0° to 180° and maintaining the geometry of both imperfections constant. The results are shown in

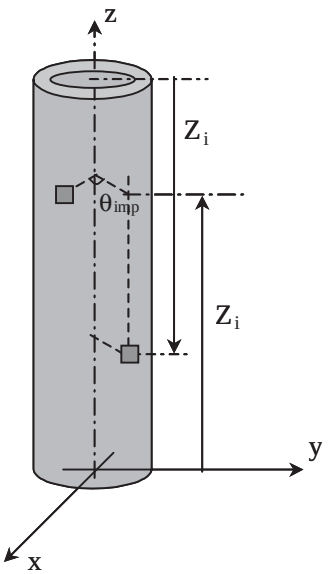

Figure 18. Position of the two local imperfections.

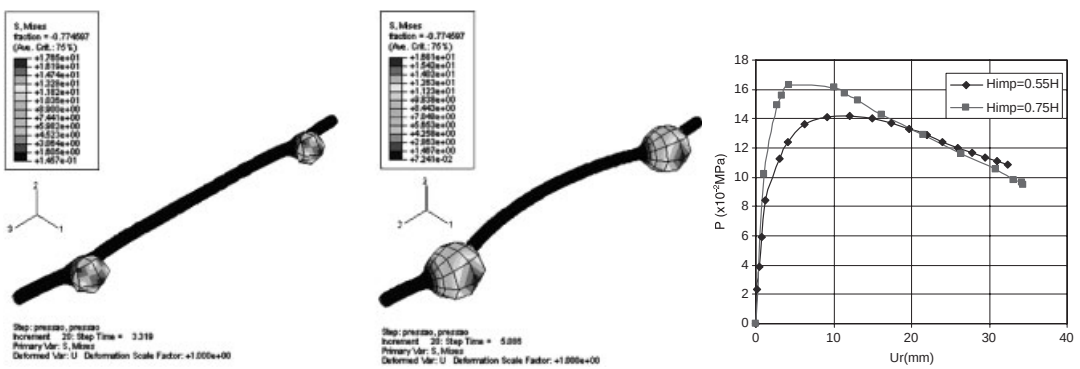

(a) H_{imp} = 0.55H (b) H_{imp} = 0.75H (c)

Figure 19. (a), (b) Deformed configurations of shells with two local imperfections forming an angle of 0° between them; and (c) respective load–displacement response.

Figures 20 and 21. θ_{imp} has a small influence on the non-linear response of the shell. However, with regard to the deformation pattern of the shell at the critical point, a puzzling fact is observed: for angles of 130°, 150° and 165°, only one bulb appears, Figures 21(e)–(g); for all other angles two bulbs are observed. It must be pointed out that the formation of two bulbs was not observed in the experiments. In the laboratory it is impossible to generate two exactly equal imperfections. Even small variations in the position and size of the imperfections, apart from other inherent model imperfections, are sufficient to localize the instability at only one position.

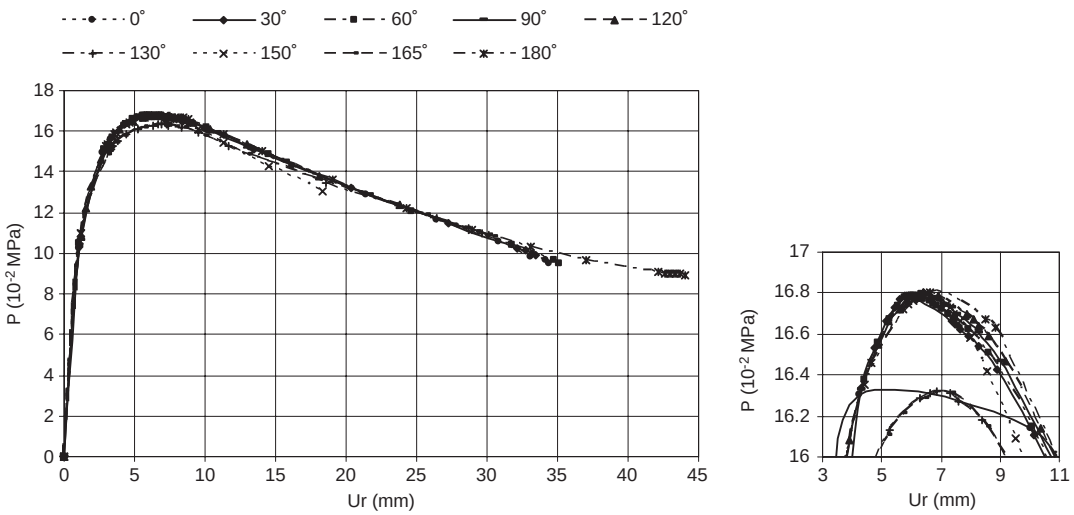

Figure 20. Variation of the internal pressure as a function of the maximum radial displacement for different values of θ_{imp}. $H_{\text{imp}} = 0.75H$.

5. INFLUENCE OF THE INITIAL CURVATURE OF THE SHELL

Finally the effect of a global imperfection on the non-linear behaviour and load carrying capacity of the shell is studied. The imperfection takes the form of a non-zero curvature in the axial direction of the shell. Positive and negative initial curvatures are considered, as illustrated in Figure 22. The positive and negative curvature is generated through ABAQUS by using a spline through three given points, namely the extremities of the shell, $(R, L/2)$ and $(R, -L/2)$, and the point located at the middle height of the shell $(x = 0)$ and radial co-ordinate $r = R \pm \Delta R$, and ΔR equals to 0.5, 1.0 and 1.5 mm. The inner and outer surface of the shell are subjected to the same curvature.

Initially, the behaviour of three shells of distinct thicknesses is analysed, considering two positive radius of initial curvature. Later two negative radius of curvature for the same shells are considered.

5.1. Influence of positive initial curvature

A numerical study of the behaviour of shells with positive initial radius of curvature of $r_1 = +0.5, +1.0 + 2.0 \times 10^4$ mm is carried out considering shells with undeformed thicknesses $H = 1.0$, 2.0, and 3.0 mm. The cylindrical shell of reference (without imperfection) has a radius of $R = 9.0$ mm and an undeformed length of $L = 300$ mm and is submitted to an initial traction of $\Delta L/L = 0.16$.

Figure 23 shows the variation of the internal pressure with the maximum radial displacement for shells with initial thicknesses of 2.0 and 3.0 mm. A considerable reduction of the critical load of the shell with the increase of the initial curvature is observed for both shell thicknesses. The deformation pattern is the same found for the perfect shell, as shown in Figure 24, with one bulb in the middle of the shell.

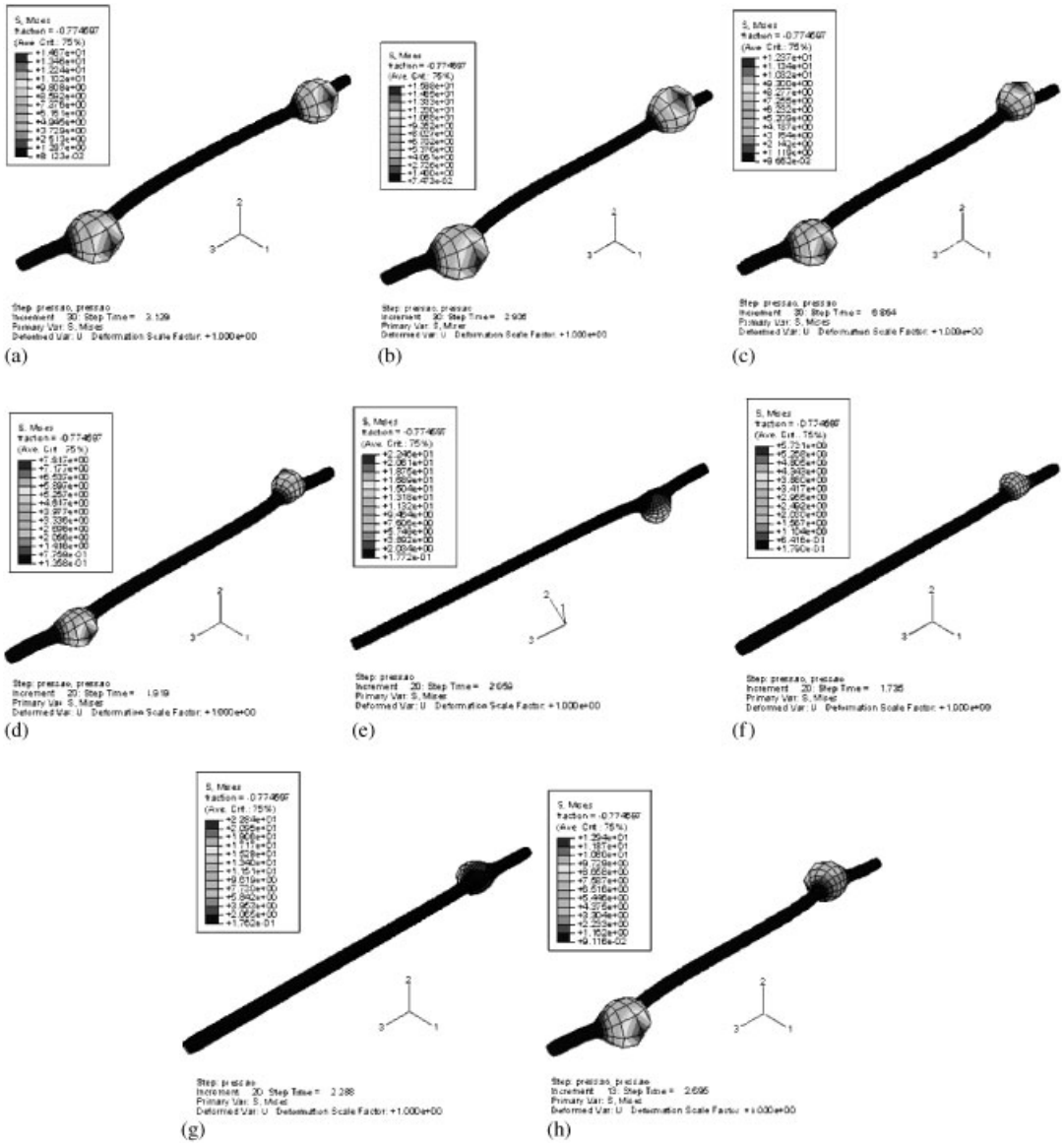

Figure 21. Deformed configurations considering two local imperfections with θ_{imp} varying from 0° to 180°: (a) $\theta_{imp} = 30°$; (b) $\theta_{imp} = 60°$; (c) $\theta_{imp} = 90°$; (d) $\theta_{imp} = 120°$; (e) $\theta_{imp} = 130°$; (f) $\theta_{imp} = 150°$; (g) $\theta_{imp} = 165°$; and (h) $\theta_{imp} = 180°$.

5.2. Influence of negative initial curvature

The same study is carried out for the geometries presented in the previous item considering now a negative initial curvature of $r_1 = -0.5$, -1.0 and -2.0×10^4 mm. Figure 25 shows the variation of the internal pressure with the maximum radial displacement for two shells. In this case, the critical

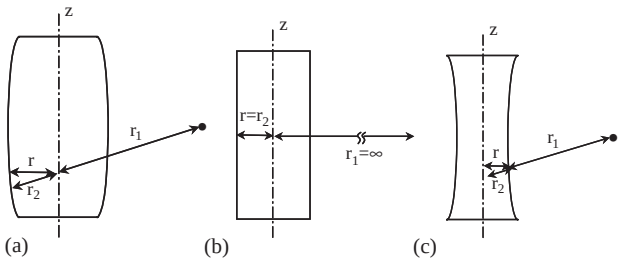

Figure 22. Representation of the initial curvature of the shell: (a) positive; (b) null; and (c) negative and its respective radius of curvature.

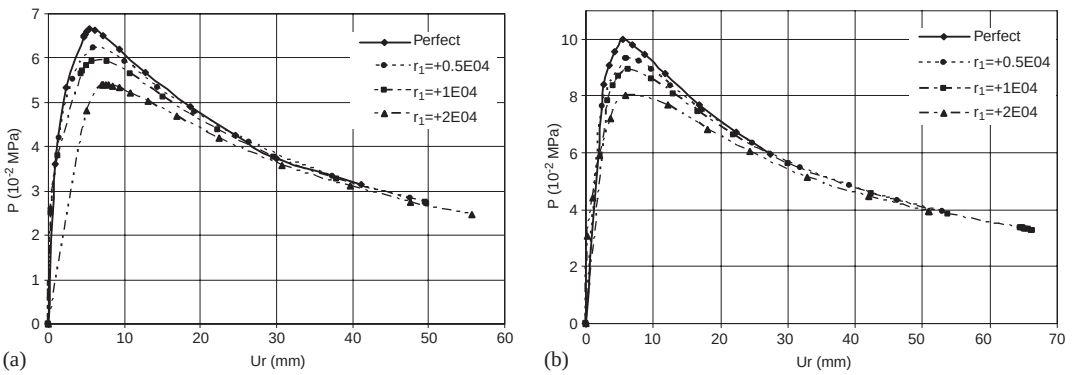

Figure 23. Non-linear response of the shell with positive initial curvature for two values of the initial thickness H and different values of the initial curvature r_1: (a) $H = 2.0$ mm; and (b) $H = 3.0$ mm.

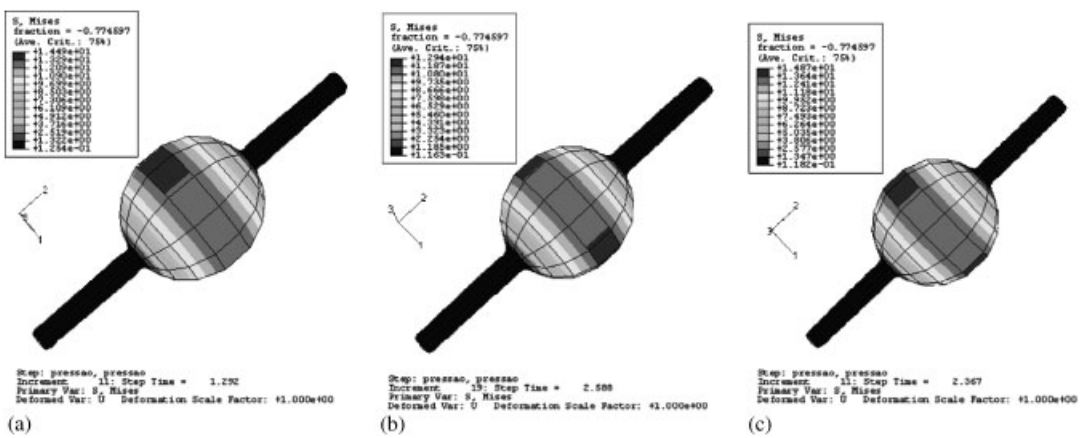

Figure 24. Critical configurations of the shell with positive initial curvature of 1×10^4 mm and thickness of 1.0, 2.0 and 3.0 mm, respectively: (a) $H = 1$ mm; (b) $H = 2$ mm; and (c) $H = 3$ mm.

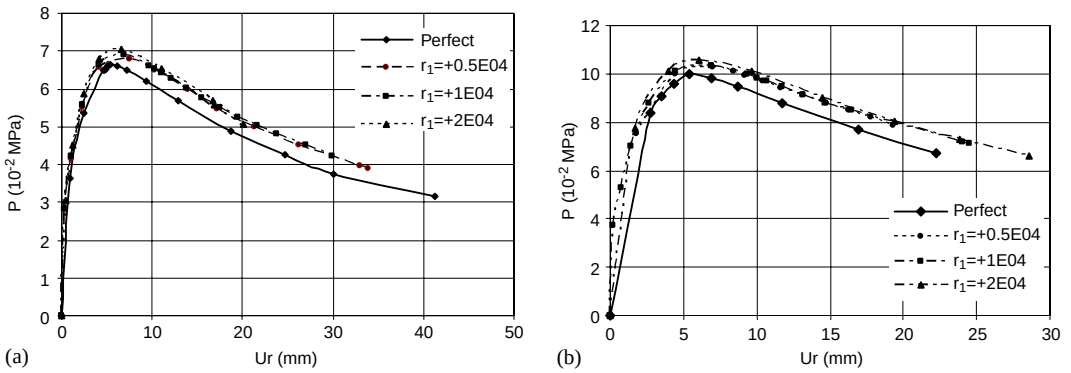

Figure 25. Non-linear response of the shell with negative initial curvature for two values of the initial thickness H and different values of the initial curvature r_1: (a) $H = 2.0$ mm; and (b) $H = 3.0$ mm.

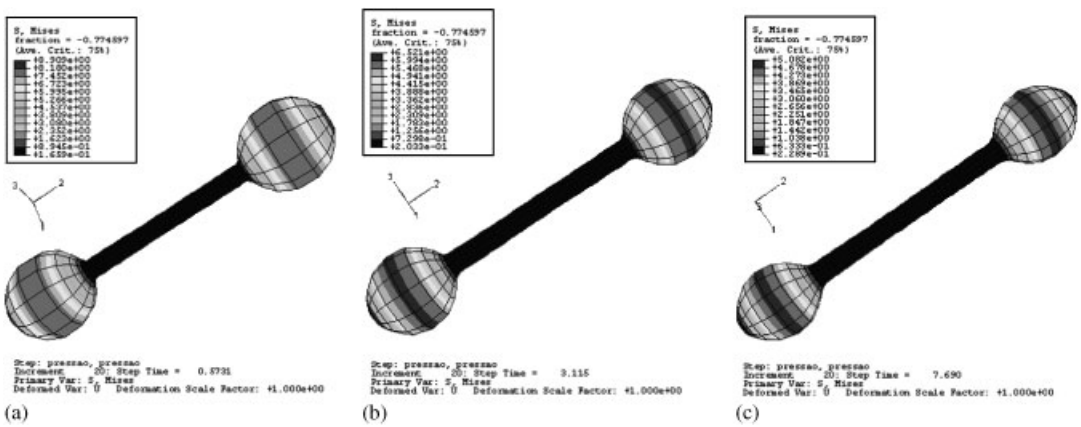

Figure 26. Critical configurations of the shell with negative initial curvature of 1×10^4 mm and thickness of 1.0, 2.0 and 3.0 mm, respectively: (a) $H = 1$ mm; (b) $H = 2$ mm; and (c) $H = 3$ mm.

load increases with increasing imperfection. Also, the critical configuration is completely different from that observed for the perfect shell, with the formation of two bulbs near the supports, as illustrated in Figure 26.

Figure 27 shows the variation of the critical pressure of the shell with the radius of curvature r_1.

6. CONCLUSIONS

The non-linear behaviour and stability of a thick hyperelastic shell under constant traction and increasing internal pressure was analysed both numerically and experimentally. In the numerical analysis, the material of the shell was modelled as a Mooney–Rivlin material with two elastic constants and the shell was discretized by the finite element method using shell elements for large

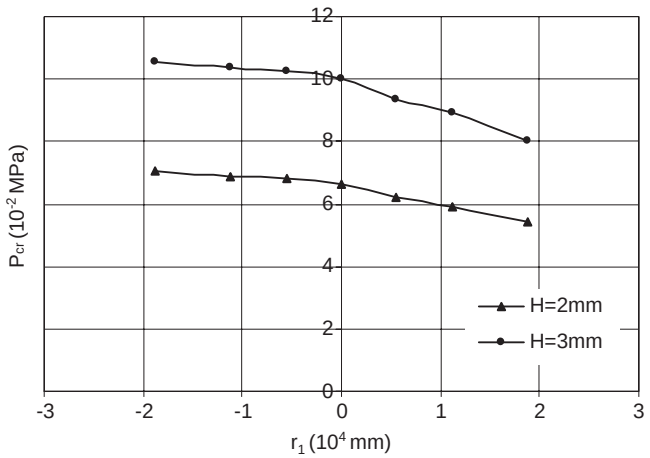

Figure 27. Variation of the internal critical pressure of the shell with initial radius of curvature (r_1) for shells with undeformed thicknesses of 2.0 and 3.0 mm.

strain analysis. The objective was to study the effects of local imperfection on the critical load and particularly on the local buckling of the shell.

First a local axi-symmetric imperfection in the form of a ring was generated through the reduction of the shell thickness. A parametric analysis of this type of imperfection was carried out varying the position, thickness and length of the imperfection. It was observed that the dimensions of the imperfection have a small influence on the critical pressure. The critical load decreases as the thickness of the shell in the region of the imperfection decreases and as the local imperfection moves away from the supports. It is also observed that the critical load is inversely proportional to the length of the imperfection. A good agreement in terms of the global behaviour was verified between the obtained numerical results and the experimental results for imperfect shells.

Another type of local imperfection in the form of a small square was analysed. A behaviour similar to the one observed previously was obtained.

The influence of multiple imperfections was also analysed. For this, two local imperfections of the same form and thickness located symmetrically in relation to the middle of the shell were considered and the angle between the two imperfections in the circumferential direction was varied between 0° to 180°. When the angle between the imperfections varied between 0° and 120° and 165° and 180° two bulbs were observed in the numerical analysis. For angles between 120° and 165°, only one bulb was observed. However, in all experiments involving two imperfections only one bulb can be observed. This can be explained by the fact that in the experimental analysis is practically impossible to generate two identical local imperfections. Even small variations in the local imperfection make the bulb to form in only one location.

Finally, a global imperfection was generated through modifications in the initial curvature of the shell in the axial direction. It was observed that, for negative initial curvatures, the critical pressure suffers a small increase in relation to the one obtained for the cylindrical shell with constant radius. On the other hand, for positive initial curvatures the critical pressure decreases as the curvature increases.

This work is part of an ongoing research on the stability analysis of thick hyperelastic shells under various loadings with emphasis on the local and global instability phenomena. The ultimate

goal of this research is to model and understand the formation of aneurysm in arteries. At the moment more refined constitutive laws are being tested both numerically and experimentally [22, 23].

ACKNOWLEDGEMENTS

This work was sponsored by the Brazilian research agencies CNPq and CAPES.

REFERENCES

1. Pamplona D, Gonçalves PB, Davidovich M, Weber HI. Finite axisymmetric deformations of an initially stressed fluid-filled cylindrical membrane. *International Journal of Solids and Structures* 2001; **38**:2033–2047.
2. Pamplona DC, Gonçalves PB, Lopes SRX. Finite deformations of cylindrical membrane under internal pressure. *International Journal of Mechanical Sciences* 2006; **48**:683–696.
3. Koiter WT. On the stability of elastic equilibrium. *Ph.D. Thesis*, University of Delft, 1945.
4. Tvergaard V, Needleman A. On the localization of buckling patterns. *Journal of Applied Mechanics* (ASME) 1980; **47**:613–619.
5. Kyriakides S, Chang YC. The initiation and propagation of a localized instability in an inflated elastic tube. *International Journal of Solids and Structures* 1991; **27**:1085–1111.
6. Green E, Adkins JE. *Large Elastic Deformations and Non-Linear Continuum Mechanics*. Oxford University Press: Oxford, 1960.
7. Mooney M. A theory of large elastic deformations. *Journal of Applied Physics* 1940; **11**:582–592.
8. Rivlin RS. Large elastic deformations of isotropic materials: I. Fundamental concepts. II. Some uniqueness theorems for pure homogeneous deformation. *Philosophical Transactions of the Royal Society of London Series A* 1948; **240**:459–508.
9. Alexander H. Tensile instability of initially spherical balloons. *International Journal of Engineering Sciences* 1971; **9**:151–162.
10. Ratner AM. Tensile stability of cylindrical membranes. *International Journal of Non-Linear Mechanics* 1983; **18**:133–147.
11. Haseganu EM, Steigmann DJ. Theoretical flexure of a pressurized cylindrical membrane. *International Journal of Solids and Structures* 1994; **31**:27–50.
12. Haughton DM. Axially elastic membranes subjected to fluid loads. *IMA Journal of Applied Mathematics* 1996; **56**:303–320.
13. Gent AN. Elastic instabilities in rubber. *International Journal of Non-Linear Mechanics* 2005; **40**:165–175.
14. Pamplona D, Bevilacqua L. Large deformations under axial force and moment load of initially flat membranes. *International Journal of Non-Linear Mechanics* 1992; **27**:639–650.
15. Tang D, Chung Y, Huang Y, Ku DN. Wall stress and strain analysis using three-dimensional thick-wall model with fluid–structure interactions will be blood flow in carotid arteries with stenoses. *Computers and Structures* 1999; **72**:341–356.
16. Haussy B, Ganghoffer J. An orthotropic hyperelastic model of cylindrical thick shells under pressure: application to the modeling of aneurysm. *15th ASCE Engineering Mechanics Conference*, New York, 2002.
17. Haughton DM, Ogden RW. Bifurcation of inflated circular cylinders of elastic material under axial loading—exact theory for thick-walled tubes. *Journal of the Mechanics and Physics of Solids* 1979; **27**:489–512.
18. Hibbit, Karlsson, Sorensen. *ABAQUS Standard Theory Manual*. *Version 6.2*. 2001.
19. Hibbit, Karlsson, Sorensen. *ABAQUS Standard User's Manual*. *Version 6.2*. 2001.
20. Xavier SR. Nonlinear behaviour and instability of hyperelastic membranes and shells. *D.Sc. Thesis*, Pontifical Catholic University, PUC-Rio, Rio de Janeiro, Brazil, 2003.
21. Treolar LRG. *The Physics of Rubber Elasticity*. Oxford University Press: Oxford, U.K., 1975.
22. Holzapfel GA, Gasser TC. A new constitutive framework for arterial wall mechanics and a comparative study of material models. *Journal of Elasticity* 2000; **61**:1–48.
23. Sokolisa DP, Boudoulas H, Karayannacos EP. Assessment of the aortic stress–strain relation in uniaxial tension. *Journal of Biomechanics* 2002; **35**:1213–1223.